



**Universiteit Utrecht**

**Beam hardening correction in multi-spectral  
mammography**

**Cyrano Chatziantoniou**  
4115120

Supervisors

Dr. Andre Mischke

Dr. John Idarraga

A thesis presented for the degree of:  
Bachelor of Science.

January 2016

### **Abstract**

Beam hardening is a phenomenon that distorts images taken with a non-monochromatic X-ray source. This report discusses the development of a correction for these distortions. The correction is part of a C++ application that uses spectral information to better detect early stages of breast cancer with X-ray imaging. First a correction using a single flat field image was completed to study the effects of correcting with such images. Afterwards a signal to thickness conversion was developed that made use of multiple flat field images. This final correction method offered interactive possibilities for the user. The code was developed by separating functionality into different modules. Whilst these modules deliver correct results, areas of improvement have been identified. The signal to thickness conversion shows some improvement over flat field correction, but the process still needs some refining as it currently uses linear interpolation.

---

## Contents

<b>1</b>	<b>Introduction</b>	<b>4</b>
1.1	X-ray imaging . . . . .	4
1.2	The Medipix3Rx detector . . . . .	5
1.2.1	Charge summing . . . . .	5
1.2.2	Spectral imaging . . . . .	6
1.3	Spectral Mammography . . . . .	6
<b>2</b>	<b>Theory</b>	<b>7</b>
2.1	Interaction between X-rays and matter . . . . .	7
2.1.1	Photoelectric effect . . . . .	7
2.1.2	Photon scattering . . . . .	8
2.2	Beam hardening . . . . .	8
<b>3</b>	<b>Corrections</b>	<b>10</b>
3.1	Flat Field Correction . . . . .	10
3.2	Beam hardening correction . . . . .	11
<b>4</b>	<b>Experimental Setup</b>	<b>15</b>
4.1	Application . . . . .	15
4.1.1	Saving data . . . . .	16
4.1.2	Flat field correction . . . . .	16
4.1.3	Signal to thickness conversion . . . . .	16
4.1.4	User Input . . . . .	17
<b>5</b>	<b>Results</b>	<b>19</b>
5.1	Images . . . . .	19
5.2	Analysis . . . . .	19
5.2.1	Leaf . . . . .	20
5.2.2	Flower . . . . .	23
5.2.3	Composition . . . . .	26
<b>6</b>	<b>Conclusion</b>	<b>29</b>
6.1	Discussion . . . . .	29

## 1 Introduction

Breast cancer is a leading cause of death among women. Early detection may allow better treatment and is thus vital in preventing deaths caused by the disease. During early stages of the disease, when no tumor is visible yet, small clusters of calcium, called microcalcifications, can give away increased cell activity [1]. These microcalcifications can be hard to distinguish due to differences in the density of breast tissue and sizes beyond the resolution of most detectors [2]. Multi-spectral mammography may aid in this issue by discriminating based on spectral behaviour.

Recent developments in photo-lithographic techniques have led to more compact pixel areas in detectors. This allows for more functionality per pixel to be added. One instance hereof is with the Medipix3Rx, which has up to eight programmable energy thresholds per pixel and can thus be used for multi spectral imaging [3]. This detector has been developed at the European Organization for Nuclear Research, *Cern*, by the Medipix3 collaboration for use in medical imaging applications such as mammography. Using this chip, the Detector R&D group at the Dutch National Institute for Nuclear Physics and High Energy Physics, *Nikhef*, is developing an application for multi-spectral mammography. This report focuses on the development of a beam hardening correction for that application. The following paragraphs will provide a short introduction on X-ray imaging, section [1.1]; the Medipix3Rx detector, section [1.2] and the multi-spectral mammography application, section [1.3]. The beam hardening phenomenon will be discussed in section [2.2].

### 1.1 X-ray imaging

X-ray imaging has been known since the late 19<sup>th</sup> century. It is based on the property that X-ray quanta, which typically have energies between 1 and 100 keV, have a much longer attenuation length than visible light. This allows imaging the non visible parts of an object, e.g. bones or the contents of a suitcase. One hundred years ago the X-rays would be converted to visible light by fluorescent materials. These days detectors similar to those in everyday digital cameras are used to detect X-rays.

As most medical facilities do not have a synchrotron to their disposal for producing monochromatic X-ray beams, the X-rays used in imaging are generated with X-ray tubes. This works by accelerating electrons toward a metal target. The electrons interact with the metal and produce photons. The photon energy depends on the energy of the electrons and of the interaction type [4]. A schematic view of an X-ray tube can be seen in figure [1].

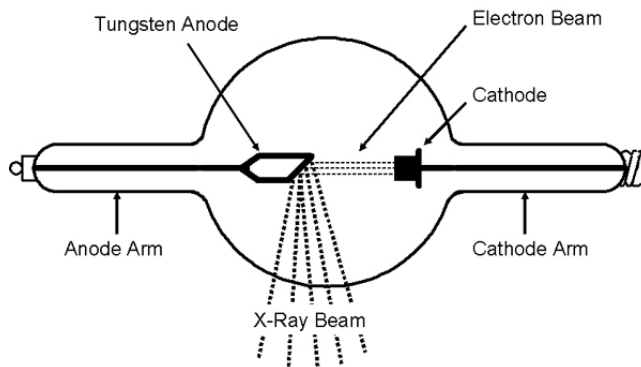


Figure 1: Schematic view of an X-ray tube. Electrons are emitted from the cathode and accelerated towards the anode where they scatter with the nuclei of the target material. Image from orau.org.

When the electron comes in proximity of a positively charged nucleus, the corresponding electric field decelerates the electron. The loss of kinetic energy is converted into a photon. This process is called

*bremstrahlung*. Since the strength of the field depends on the proximity to the nucleus, electrons that come closer to the nucleus will produce higher energy photons. The highest X-ray energy is determined by the peak voltage (kVp) of the accelerating field. When the energy of the incoming electron exceeds the binding energy of an orbital electron in the target, it can eject the atomic electron. When the vacancy is filled by an electron from a higher shell, a characteristic X-ray is produced. These are noted as  $X_y$  where the capital letter depicts the shell where the electron was ejected and the subscript letter states whether the transition was with an adjacent shell ( $\alpha$ ) or from a non-adjacent shell ( $\beta$ ). Characteristic X-rays that are not from the K-shell can be neglected, as they are almost entirely attenuated before reaching the detector. *Bremstrahlung* and the production of characteristic X-rays combine to make the spectrum of an X-ray tube. This is shown in figure [2].

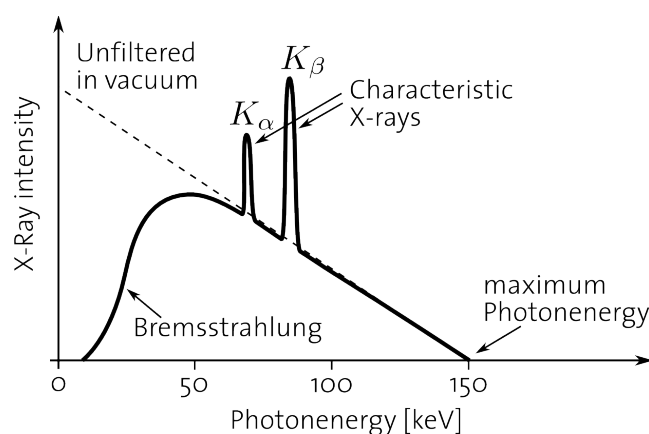


Figure 2: Spectrum of an X-ray tube of 150 kVp with the characteristic  $K_\alpha$  and  $K_\beta$  peaks. Image from: miac.unibas.ch

## 1.2 The Medipix3Rx detector

The Medipix3Rx detector is a pixel detector readout chip that can be connected to a semiconductor detector; it acts as an intermediate piece of hardware between the detector and the data output that can perform some basic tasks on the incoming signal from the detector [3]. A graphical representation is given in figure [3]. As can be seen, the detector is connected with the readout chip by a number of bonds called bump bonds. These bonds are the only way for a signal to reach the readout chip. The spacing between these bonds, called pitch, determines the resolution. The chip has 256x256 of these bonds with a pitch of 55  $\mu\text{m}$ . The pitch can also be increased to 110  $\mu\text{m}$ . When increasing the pitch, only one in four bump bonds are connected, decreasing resolution, but allowing more advanced operations on the signal of the remaining bond.

### 1.2.1 Charge summing

Whenever an X-ray quantum hits the semiconductor detector, it frees some electrical charge. The detailed description of how this happens is described in section 2.1. After being freed, the charge starts to drift towards a connection between the detector and the readout chip due to an electric field. This process can happen anywhere in the detector and there is no guarantee that all the charge will drift towards a single connection. All of the connections that receive some charge will register it as a low energy photon. This is called charge sharing. The Medipix3Rx chip prevents this by summing the charge of the neighbouring pixels each time one is triggered.

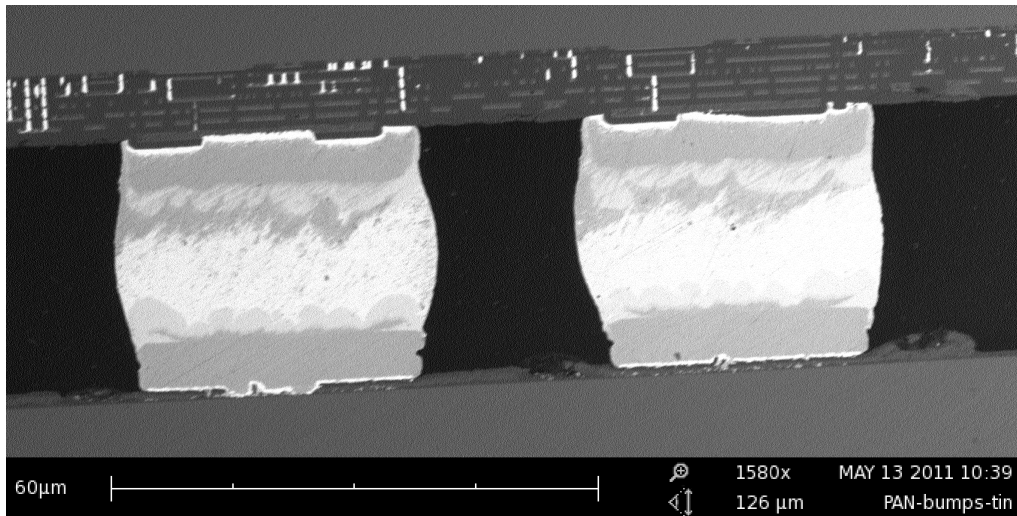


Figure 3: Cross section of the Medipix3Rx chip (top) with two bump bonds (middle) connecting the chip to the detector (bottom). The grey lines in the chip are the logic circuits. Image credit Nikhef.

### 1.2.2 Spectral imaging

The Medipix3Rx chip can impose two thresholds per pixel on the incoming signal. These thresholds can be used to look at the higher energy photons only. In the so-called colour mode, the chip can combine the thresholds from the unused parts to impose eight thresholds per pixel. This can be combined with charge summing to accurately detect photons that free charge in a large area.

## 1.3 Spectral Mammography

X-ray imaging has had many applications in the past century in many different fields. In the early days shoe-fitting fluoroscopes were used to determine how well a pair of shoes would fit someone [7]. When the dangers of exposure to the radiation became clear, many of these applications were banned. Nowadays X-ray imaging is used typically for medical purposes and security applications.

Mammography is an X-ray imaging technique specifically used for breast imaging. The principle is the same as with other imaging techniques, only the setup is altered to work with the relatively soft breast tissue. Its goal is the early detection of breast cancer by finding, amongst other things, microcalcifications. These are small calcium deposits in the mammary gland that can point to high cell activity. By looking at the amount and their shape, a radiologist can determine whether someone is at risk of developing advanced breast cancer. The small size of the microcalcifications combined with the large variance of density in the breast makes detection difficult.

When looking at the spectral behaviour of the tissue in the image, the microcalcifications can be better revealed. Figure [4] shows the attenuation of water and calcium for different energy incident photons. The spectral behaviour is the same for most of the plot: When the energy increases, the attenuation of water and calcium will lower roughly the same amount. At two points, one being is the K-edge at 4 keV and the other is a region around 50 keV, this behaviour changes. When looking at mammograms of 25, 50 and 75 keV, the attenuation differences of the microcalcifications will be distinguishable from the attenuation differences of the surrounding tissue.

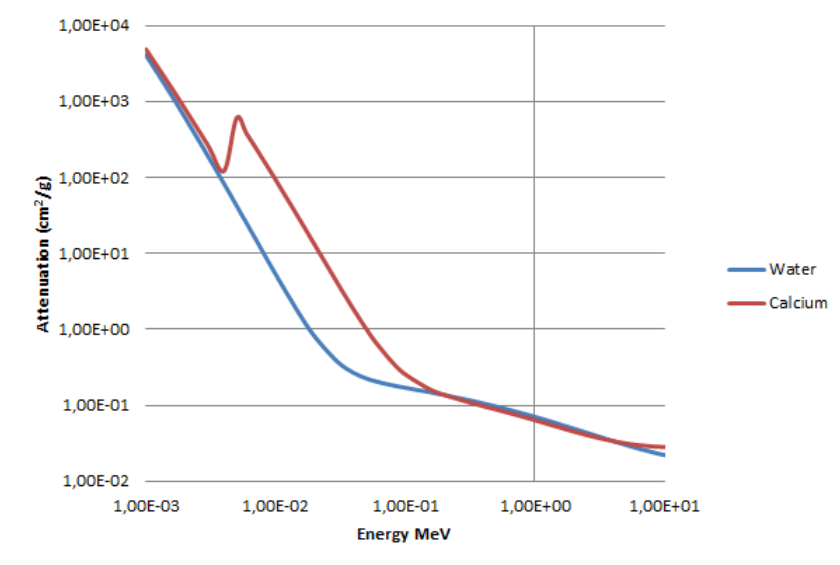


Figure 4: Attenuation of water and Calcium plotted as a function of photon energy. Data taken from physics.nist.gov.

## 2 Theory

The detection of the x-rays is a result of photon-matter interactions. This section will treat some of the theory behind these interactions. As this is a report and not a textbook, a lot will not be covered. The interested reader is referred to other literature [9] [10].

### 2.1 Interaction between X-rays and matter

When a photon interacts with an atom, its energy is either absorbed completely or partially in the case of scattering. When a beam of electromagnetic waves collides with something, the absorption and scattering of photons cause the beam to be attenuated. The interactions are dictated by a host of different effects. These effects contribute to the total attenuation, although the contribution differs for each effect depending on the energy of the X-rays.

At a certain energy, a beam with intensity  $I_0$  that passes through a layer of matter with density  $p$ , thickness  $x$  will emerge with intensity  $I$  with:

$$\frac{I}{I_0} = e^{-(\mu p)x}. [8] \quad (1)$$

Here  $\frac{\mu}{p}$  is called the mass attenuation coefficient. It is related to the different attenuation effects by:

$$\frac{\mu}{p} = \frac{\sigma_{tot}}{uA}. \quad (2)$$

Here  $u$  is the unit of atomic weight and  $A$  is the atomic mass of the material.  $\sigma_{tot}$  is the total cross section of the different effects. In theory, there are 12 ways in which photons can be absorbed or scattered [9]. In the energy range of 1-100 keV the attenuation can be mainly attributed to the photoelectric effect and Compton scattering.

#### 2.1.1 Photoelectric effect

Atomic electrons can completely absorb incoming photons. During this process, if the photon energy is higher than the binding energy between the electron and the nucleus, the electron will be ejected. The

higher the binding energy between the electron and the nucleus, the higher the chance of absorption. Roughly 80 % of the absorption occurs in the K-shell, provided the X-rays exceed the binding energy. For instance, in aluminum this binding energy is 1559.6 eV [11].

Due to conservation of momentum, free electrons can not completely absorb photons and will instead scatter them.

### 2.1.2 Photon scattering

If the energy of an incoming photon is very low, it can scatter elastically. For energies approaching the electron mass (0.51 MeV), the photon momentum can not be neglected and the scattering is inelastic with the electron absorbing some of the energy. This process is called Compton scattering. If the scattered photon has high enough energy, the whole process repeats until the photon eventually gets absorbed via the photoelectric effect, or leaves the material.

## 2.2 Beam hardening

When looking at the total attenuation in figure [5], one can clearly see an energy dependence: higher X-ray energies get attenuated less. A non-monochromatic beam that passes through matter will thus have less low energy X-rays, resulting in a *harder* beam. An example of this can be found in figure [6]. Here an X-ray spectrum is being hardened with different aluminum plates.

The hardening of an X-ray beam in itself is not really a problem in imaging; there might be a reduced contrast in the softer structures of the sample. A problem arises, however, in the detection of the X-rays. This detection is also energy dependent and furthermore the energy dependence is unique for each pixel. This causes noise-like artifacts in the image, decreasing its quality. A correction is needed to remove these artifacts.

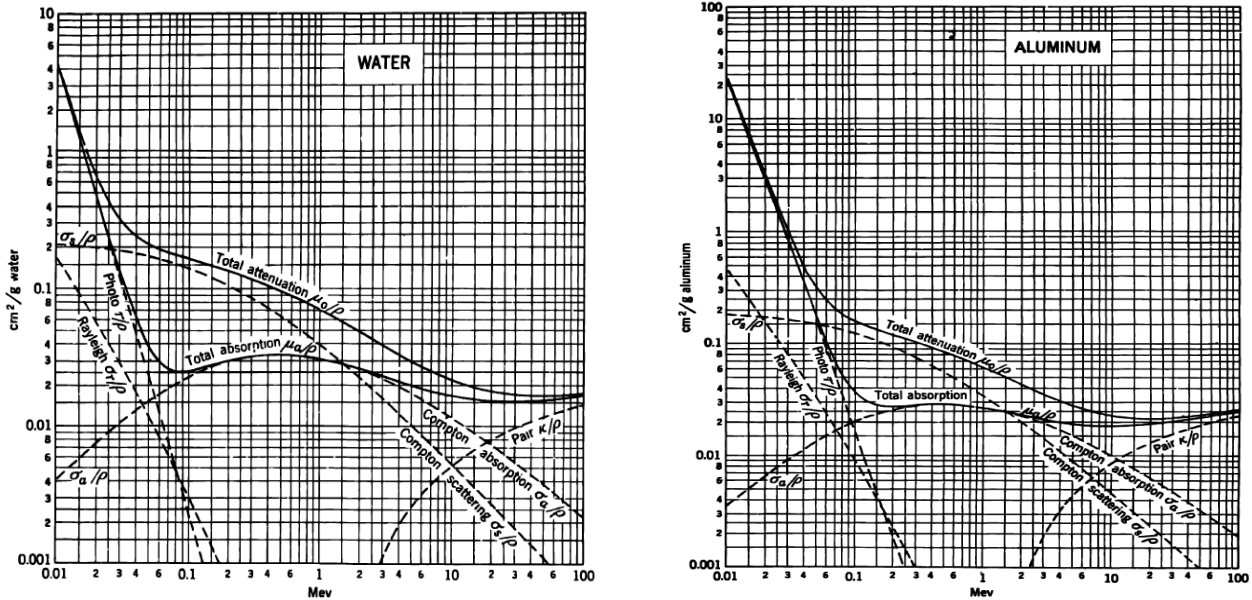


Figure 5: Absorption and attenuation plotted against photon energy for water (left) and Aluminum (right). The region of interest is at energies between 0.01 and 0.1 MeV. Here the photoelectric effect and Compton scattering are dominant with minor influences from Rayleigh scattering and Compton absorption. Image taken from [10].



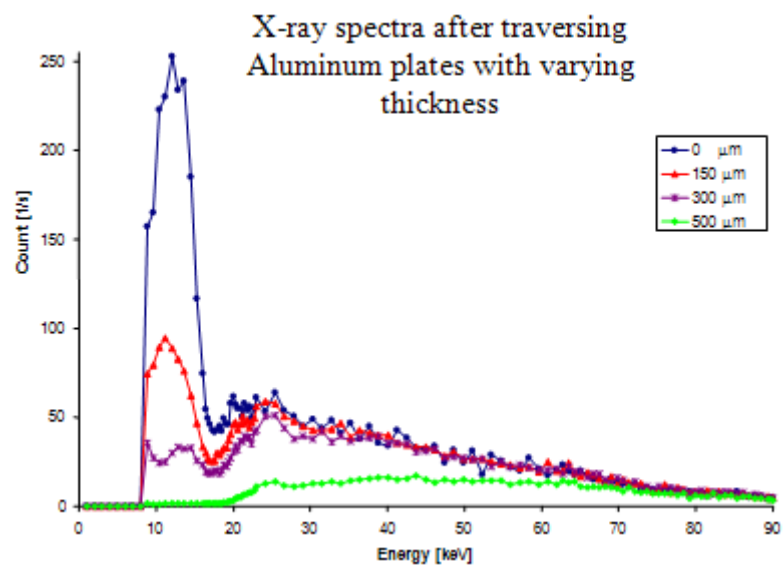


Figure 6: X-ray spectrum of a tungsten X-ray tube at 90 kV after beam hardening with aluminum plates. Image taken from [12].

### 3 Corrections

There are a multitude of corrections that can be applied to an image: their contrast can be enhanced, their noise can be removed, over and under saturation can be reduced. This section focuses on two: the flat field correction and the signal to thickness conversion. Both of these are post processing methods, meaning that they can be applied after the image has been taken.

#### 3.1 Flat Field Correction

The signal  $s$  that is measured can be found using the mass attenuation law from equation [1]. It requires some changes to account for noise and other influences caused by the setup:

$$s = a e^{bt} + c.[6] \tag{3}$$

Here the constants  $a$  and  $b$  are related to the beam intensity and the mass attenuation. The constant  $c$  is an offset that is caused by a number of things, including photon response per pixel. When comparing the signal to an unattenuated beam, the offset can be removed. This correction is done as follows:

$$s_{new} = \ln \left( \frac{s_{original}}{s_{correction}} \right). \tag{4}$$

It is also possible to first attenuate the beam with a homogeneous sheet, hardening the beam somewhat. This increases contrast of the corrected image in the denser regions of the sample, as mostly high energy X-rays penetrate this. It also lowers contrast in the less dense regions, since most of the information there comes from the lower energy X-rays which are attenuated by the sheet. Figure [7] shows an example of this process. An image was made of a leaf, a mushroom and some berries with a 15 kVp X-ray tube and corrected with flat field image. Images (a) and (b) of the figure show the grid of adjacent Medipix3Rx chips. In the current setup, only three chips are activated. At the border of the chips the detector area corresponding to a bump bond is larger; increasing the amount of X-rays that are registered at those sites. This can be seen in the image two lines between the chips. It is a typical example of an offset that can be corrected for.

A good way to analyse the result of a correction is to look at the image histogram, such as the one shown in figure [7 (d)]. This shows the distribution of the grey values in the image. The result of flat field corrections can be seen by comparing histograms of the images. Three histograms corresponding to corrections made with aluminum layers of 0, 100 and 1000  $\mu m$ , are analysed in figure [9]. The original histogram contained two peaks; by splitting the histogram, each peak can be looked at with more detail. The figure shows that there is a very clear decrease in the contrast of the softer structures when corrected with a harder beam as well as a slight increase in contrast of the denser structures when corrected with a harder beam.

### 3.2 Beam hardening correction

The effect of beam hardening can be removed from the image by means of a signal to thickness conversion. To do this, a number of flat field images are made; each attenuated by a sheet with a certain thickness. The more the material of the sheet resembles the sample that is being imaged, the more any artifacts are removed. When plotting the signals of each of these images against the thickness of the sheet, a relation can be found. An example of this is illustrated in figure [8].

Finding the relation from the data can be done by inverting the mass attenuation law and getting an expression for the thickness. By means of fitting the expression through the data, or by interpolating numerically, any signal within range can be converted to a thickness. In this project, the numerical method has been chosen. This is due to the fact that numerical interpolation is less time consuming to implement and that it was expected that the results of the two methods would be similar.

This technique works better for removing beam hardening artifacts than just the open beam correction because it uses the information of the correction which best matches the sample for each pixel. When there are areas of both high and low attenuation in a sample, an open beam correction would only remove artifacts in one of the two areas, whereas a beam hardening correction can remove artifacts in both areas.

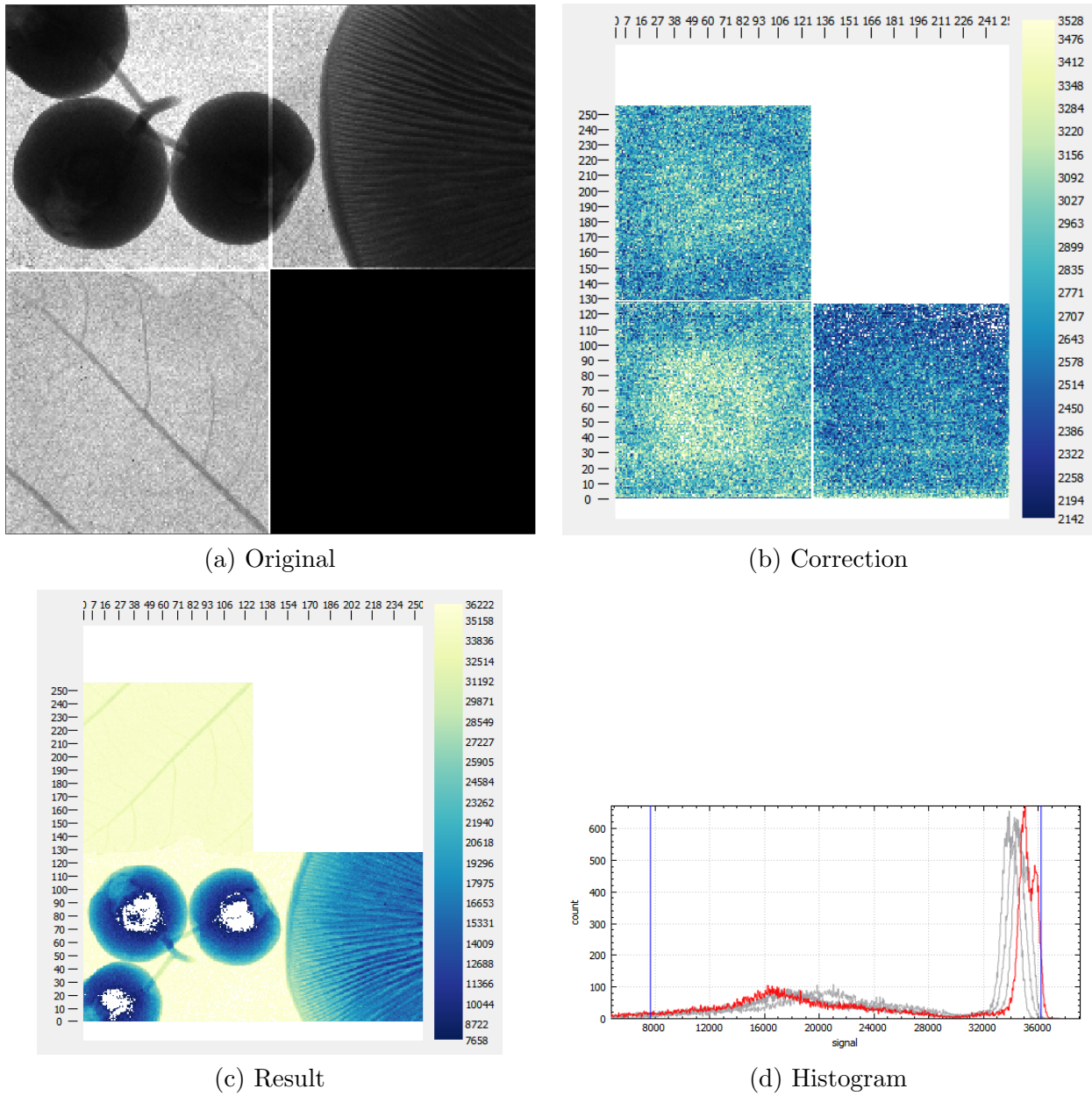


Figure 7: Open beam correction process demonstrated on a composition of a leaf, a few berries and a mushroom. Image made with a 15 kVp 40 mA beam. (a) Shows the original image, (b) shows the  $0 \mu\text{m}$  correction layer, (c) shows the image after the correction is applied and (d) shows the histogram of the result. The histogram consists of one sharp peak that corresponds to the leaf and other soft structures, as well as one broad peak that corresponds to the denser structures, such as the berries or the mushroom.

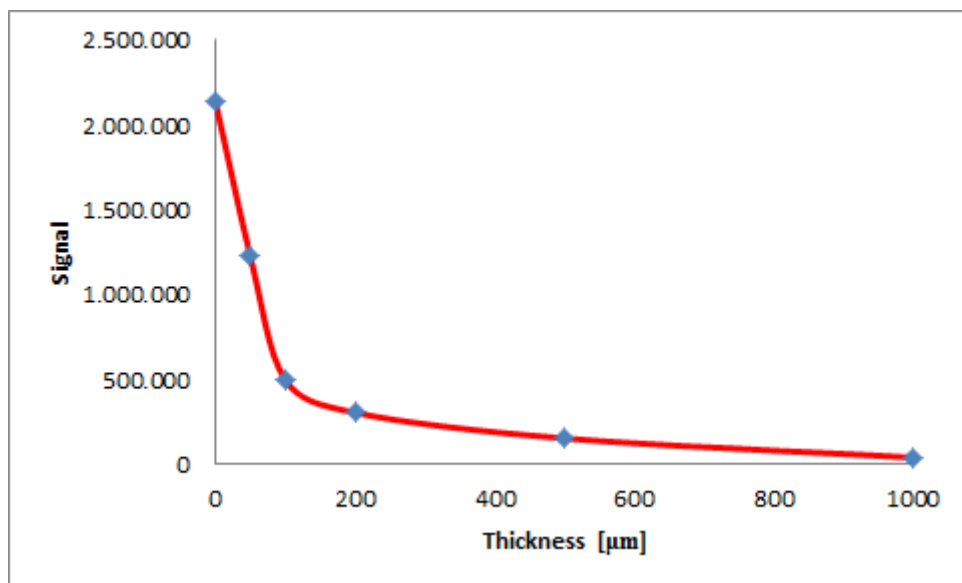


Figure 8: Averaged signal of flat field image that was attenuated by aluminum sheets versus sheet thickness (blue markers), together with signal to thickness relation (red line). The images were made with a 15 kVp 40 mA beam. The exponential decay of the signal is in accordance with the mass attenuation law from equation 1.

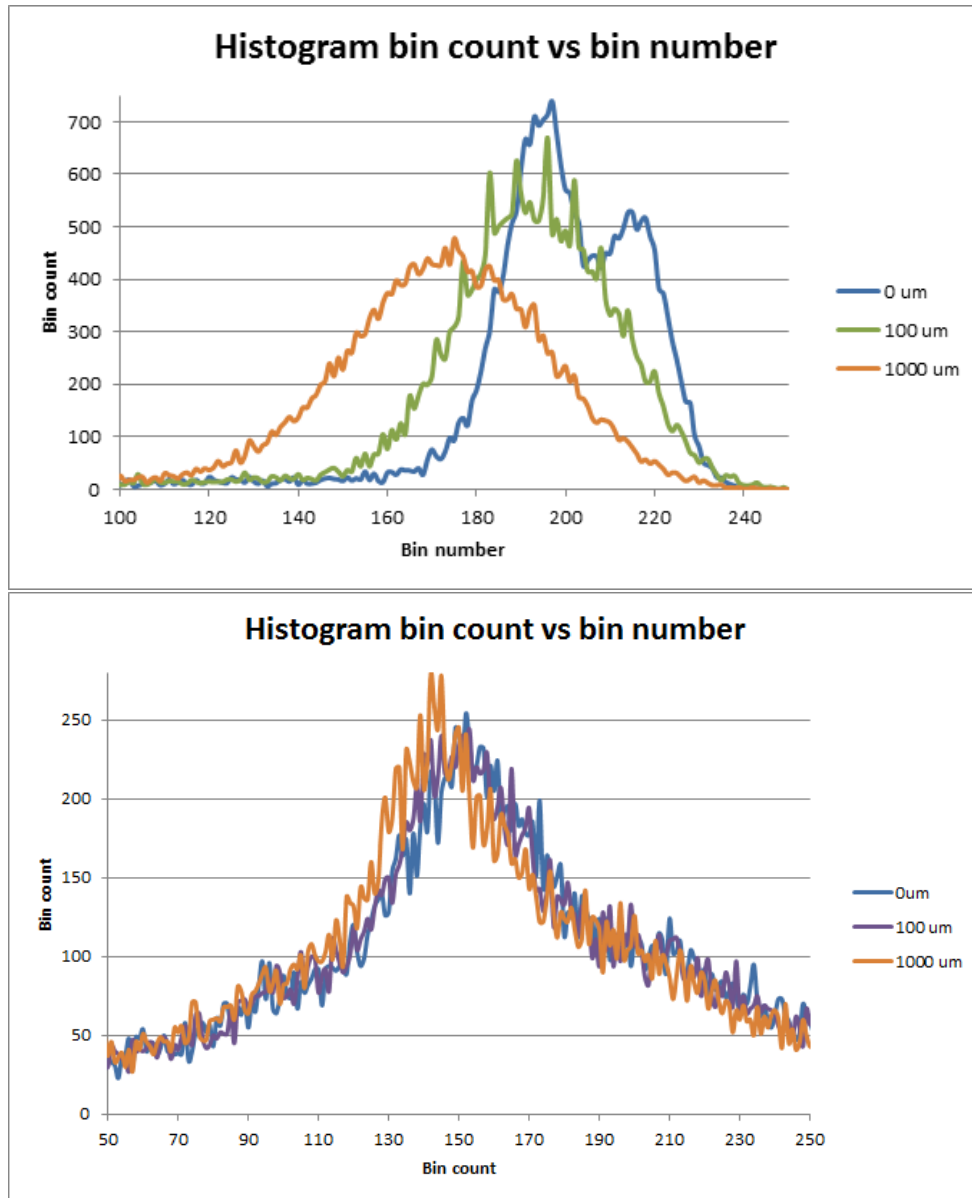


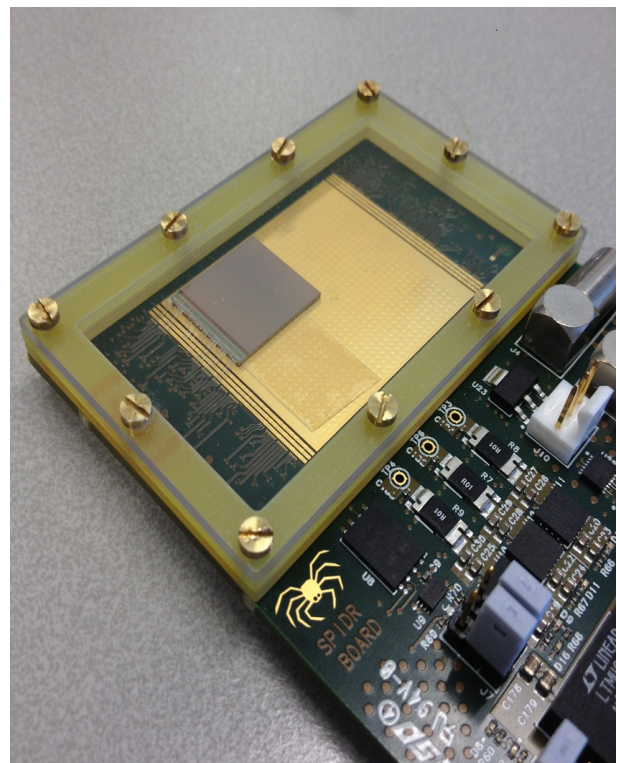
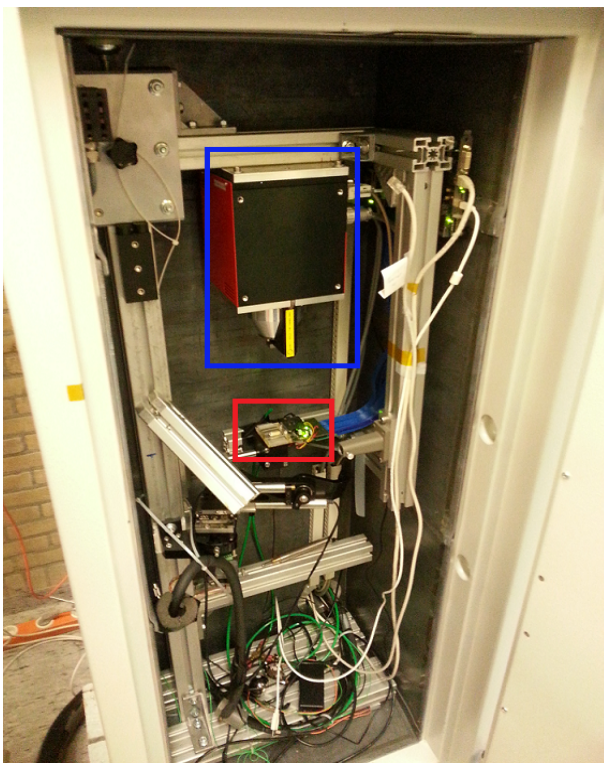
Figure 9: Analysis of the histogram of the images produced by open beam corrections made with aluminum layers of 0, 100 and 1000  $\mu\text{m}$ . Top: part of the histogram corresponding to the sharp peak in figure 7. Bottom: part of the histogram corresponding to the broader peak in figure 7. The shift of the peak is caused by the ranges of the partial histograms not being the same.

## 4 Experimental Setup

The images for this report have been made using a 99 kVp Tungsten target X-ray tube at Nikhef. They were made with four Medipix3Rx chips in a grid, which are connected to a computer running software that was specifically developed for spectral mammography. This setup is shown in figure [10a]

The X-ray tube emits a signal that is detected by four Medipix3Rx chips. These chips are placed in a special module called the Spidr, short for *Speedy Pixel Detector Readout* module. Spidr has been developed by Nikhef to be able to readout pixel detectors [5]. Figure 10b shows the Spidr module with one Medipix3Rx chip. The module can hold up to four Medipix3Rx chips. When the images for this report were taken, it was only possible to read three of the chips.

Communication with the software is possible via a *Field Programmable Gate Array*, FPGA, which has a micro controller that allows instructions to be sent by the computer via TCP and data to be sent to the computer via UDP.



(a) Overview of the X-ray setup. Blue: The X-ray tube. Red: The Spidr module. (b) Close up of the Spidr module holding a single Medipix3Rx chip. Image credit Nikhef.

### 4.1 Application

The application is written in C++ using Qt libraries. Qt is a set of libraries for C++ that are specialized for producing graphical interfaces and cross platform development [13]. The application is made to run on the major operating systems. A screenshot of the application is shown in figure [11]. The main part of the application was already developed. During the scope of this project a number of features were added. These are described in the following paragraphs.

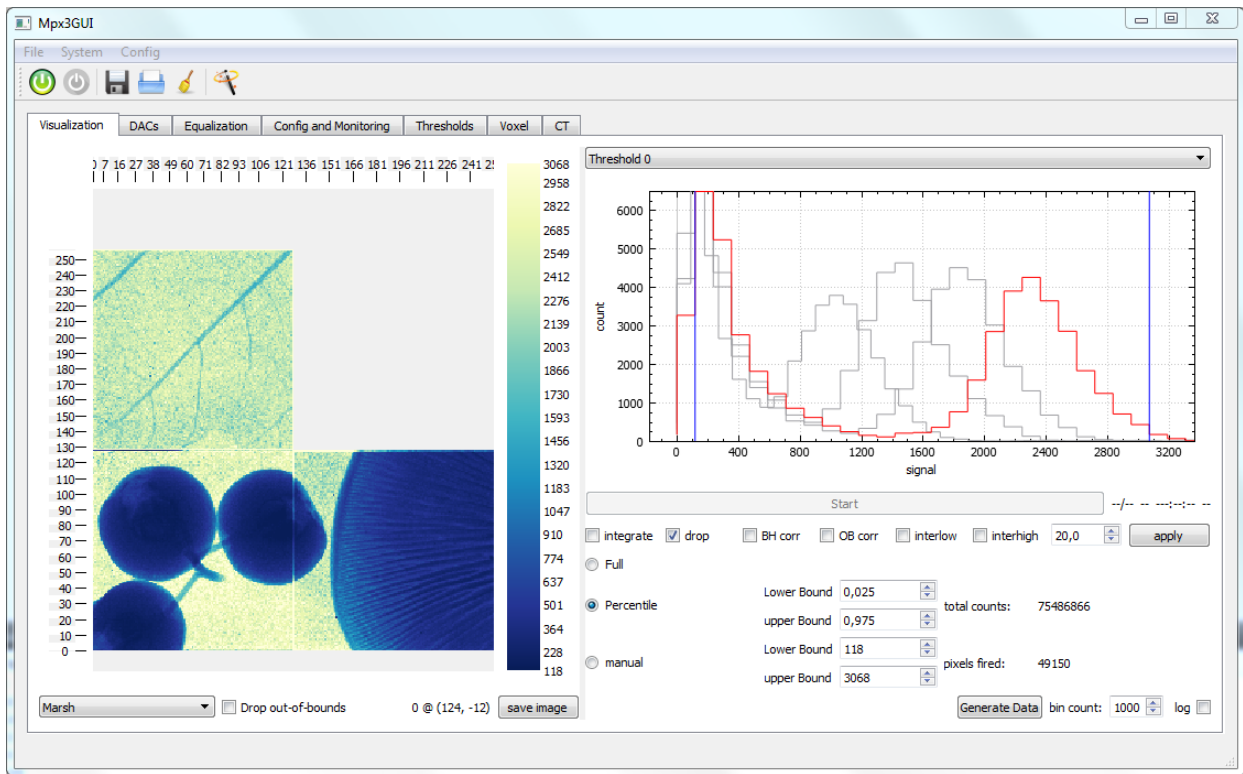


Figure 11: The spectral mammography application. On the left the image is shown. On the right the histograms corresponding to the different energy thresholds are plotted.

#### 4.1.1 Saving data

The application had a way to save the data which used the internal memory structure of the software and exported to .bin files. These files could not be read by any conventional image processing programs, making the analysis of the produced images a lot harder. To solve this, the software was changed to also save the signal of each pixel as numeric values in a .txt file.

#### 4.1.2 Flat field correction

The flat field correction was already partially implemented, but still needed to be altered to produce integer values for each pixel. To do this, first the pixel with value closest to zero was found. Then the amount of digits before the first non-zero number,  $n$ , was noted. All other pixels were multiplied with  $10^n$ , effectively shifting all the decimal places. As discussed in section 3.1, the correction involves taking the logarithm of the fraction of the original image and the correction image. This allows for negative numbers, that make sense physically, but not graphically. This was corrected by taking the lowest result and using it as an offset for all the others.

#### 4.1.3 Signal to thickness conversion

To apply the signal to thickness conversion, the user has to perform a number of actions. Therefore, a graphical interface had to be created. This is shown in figure [12]. The main purpose of the window is creating a list of flat field correction images that will be used to apply the signal to thickness conversion.



The program starts with an empty list to which the user can add items containing the thickness and the material of the sheet that were used to make the flat field correction. Selecting an item allows the user to load data, or take data using an X-ray tube and the Medipix3Rx chip. Pressing the *start* button then starts the signal to thickness conversion process. The window also plots the total signal against the thickness for each of the layers, making a crude signal to thickness plot which serves as feedback for the user.

The correction is applied by accessing all the correction layers that the user loaded or created and storing the signal of each pixel into a *vector* for that pixel. The term *vector* here refers to the C++ data structure, not to the mathematical definition. Once all the *vectors* have been filled, the program reads the signal of a pixel in the original image and interpolates it using the *vector* corresponding to that pixel. This process is repeated for each threshold. To do the interpolation, an open source library that makes use of the spline cubic interpolation algorithm, was used [14]. While testing, it was discovered that this interpolation method did not work well with exponential functions. The current solution is to interpolate linearly.

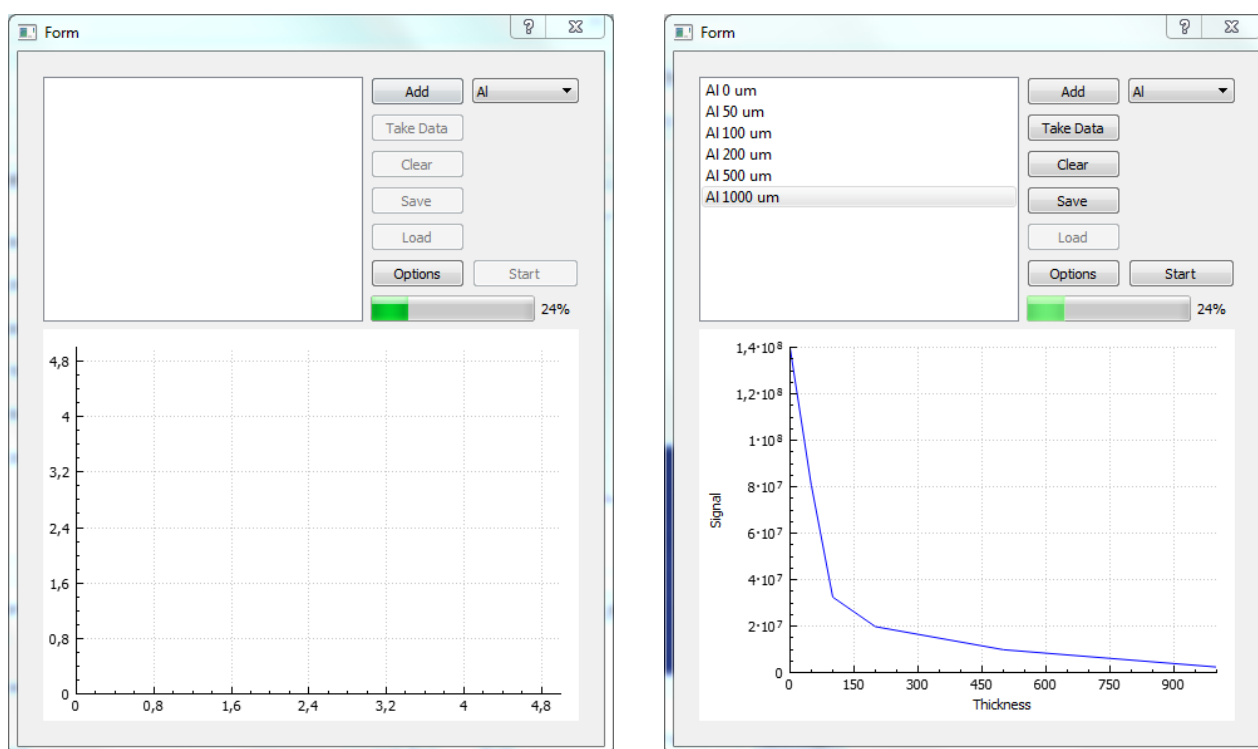


Figure 12: Graphical User Interface for the signal to thickness conversion. The left image shows the interface right after it's created, the right image shows the interface after some correction layers have been added. The interface itself contains a list of correction layers, a number of buttons and a signal to thickness plot of the average of the correction layers.

#### 4.1.4 User Input

In order for the correction to work, the correction layers that the user loads have to meet a number of conditions. These might not always be intuitive to the user, or the user might accidentally disregard them. To ensure that the program does not crash due to user input, some restrictions have been placed on the actions that can be taken.

1. The interpolation algorithm needs at least three correction layers to function. This has been

realised by disabling the *start* button until at least three corrections have been loaded.

2. The interpolation algorithm needs to receive sorted values for the signal and thickness points. To prevent the user from having to insert the correction layers in order, first an attempt was made to sort all of the *vectors*. This proved to take a lot of computation and development time, so the problem was addressed differently. The different corrections are now stored in a *map*, which is a data structure that pairs each contained value with a key. By sorting only the thicknesses of the correction layers, which are identical for each pixel, and using these as keys, the data can be sorted very quickly.
3. If there is no image to apply the correction to, the program could crash while trying to read from the memory. To prevent this, the beam hardening window can only be opened if an image is loaded.
4. If the user adds corrections to the list, but does not load any data, the program will crash. To make sure that this doesn't happen, the algorithm won't start until all correction layers have been loaded correctly.
5. No two correction layers can have the exact same thickness. The interpolation algorithm won't know what to do with the duplicate values. To ensure that this does not happen, the program does not let the user add a correction layer with an existing thickness. Selecting an existing item and loading data for the second time has been disabled for the same reason, although this could be circumvented.

## 5 Results

In this section the images produced using the signal to thickness conversion are discussed. They will be compared to the original images and to the ones made with the flat field projection.

### 5.1 Images

Figure [13] shows the corrections applied to the image of a leaf, figure [15] shows a flower and figure [17] looks at a composition of a leaf, a mushroom and some berries. The histograms corresponding to each of the images are shown as well in figures [14], [16] and [18] respectively.

The images are colour scaled to show the intensity of the X-ray beam at a certain pixel. The images that were made with the flat field correction will have values that differ from the original. This is due to the offset and the shifting of the decimal places as discussed in section 3.1.

For the images produced by the signal to thickness conversion, the colour scale shows the thickness that an aluminum sample would need to be in order to attenuate the X-ray beam as much as the sample did. It is measured in microns. The reason that it shows the thickness for aluminum is that the flat field corrections have been made using aluminum.

In some cases, images show negative thicknesses. This happens because the wrong flat field corrections were used. For instance if the original image was taken using a 40 kVp beam and the flat field correction was made using a 20 kVp beam. In that case even the flat field correction made without any sheet attenuating the beam will register at a lower intensity than some pixels in the original image. The algorithm then extrapolates and finds a negative thickness. This also means that the correction will be less effective.

### 5.2 Analysis

The visual differences between a flat field correction and a signal to thickness conversion can be small. To be able to still compare the effects, histograms of the images are used. Before comparing these histograms, it is important to first look at the effect of beam hardening on a histogram.

When large parts of a sample attenuate the X-rays by the same amount, the histogram will show peaks. When beam hardening is introduced and is not corrected for, these peaks will become less sharp. This is because the pixels in the detector each react differently to different spectra, causing a spread in the signals that they produce. Sharper peaks will thus mean that the correction has worked.

One caveat while looking at the histograms: In the histograms of the original images and the images corrected using a flat field correction, higher signal will mean a thinner structure. In the histograms corresponding to the signal to thickness conversion, the signal is actually the thickness. Higher signal here means that the structure is thicker. This effectively mirrors the histograms.

### **5.2.1 Leaf**

The leaf in figure [13] consists mainly of very thin structures. Because there is little difference in thickness throughout the sample, a flat field correction performs similarly to a signal to thickness conversion. This can be seen, as visually the two corrections look the same.

Looking at the histograms in figure [14], the number of peaks increases from one at the original to two at the flat field correction to three at the signal to thickness conversion. There is also a large flat area in the histograms that corresponds to the thicker structures of the leaf. This area is slightly shorter and higher in the histogram of the signal to thickness conversion.

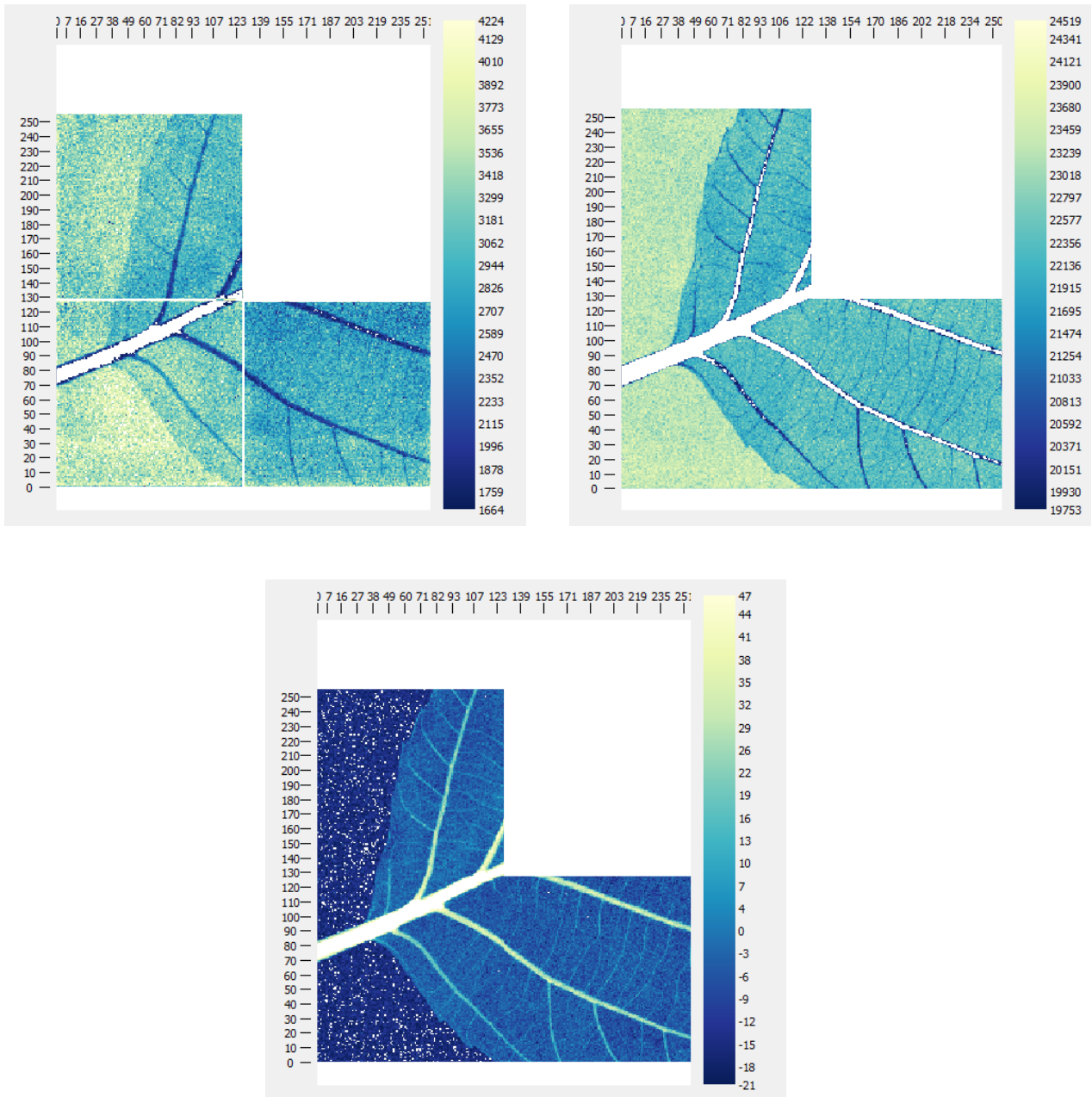


Figure 13: Comparison of corrections on X-ray image of a leaf. Top left: Uncorrected image. Top right: Result after flat field correction. Bottom: Result after signal to thickness conversion.

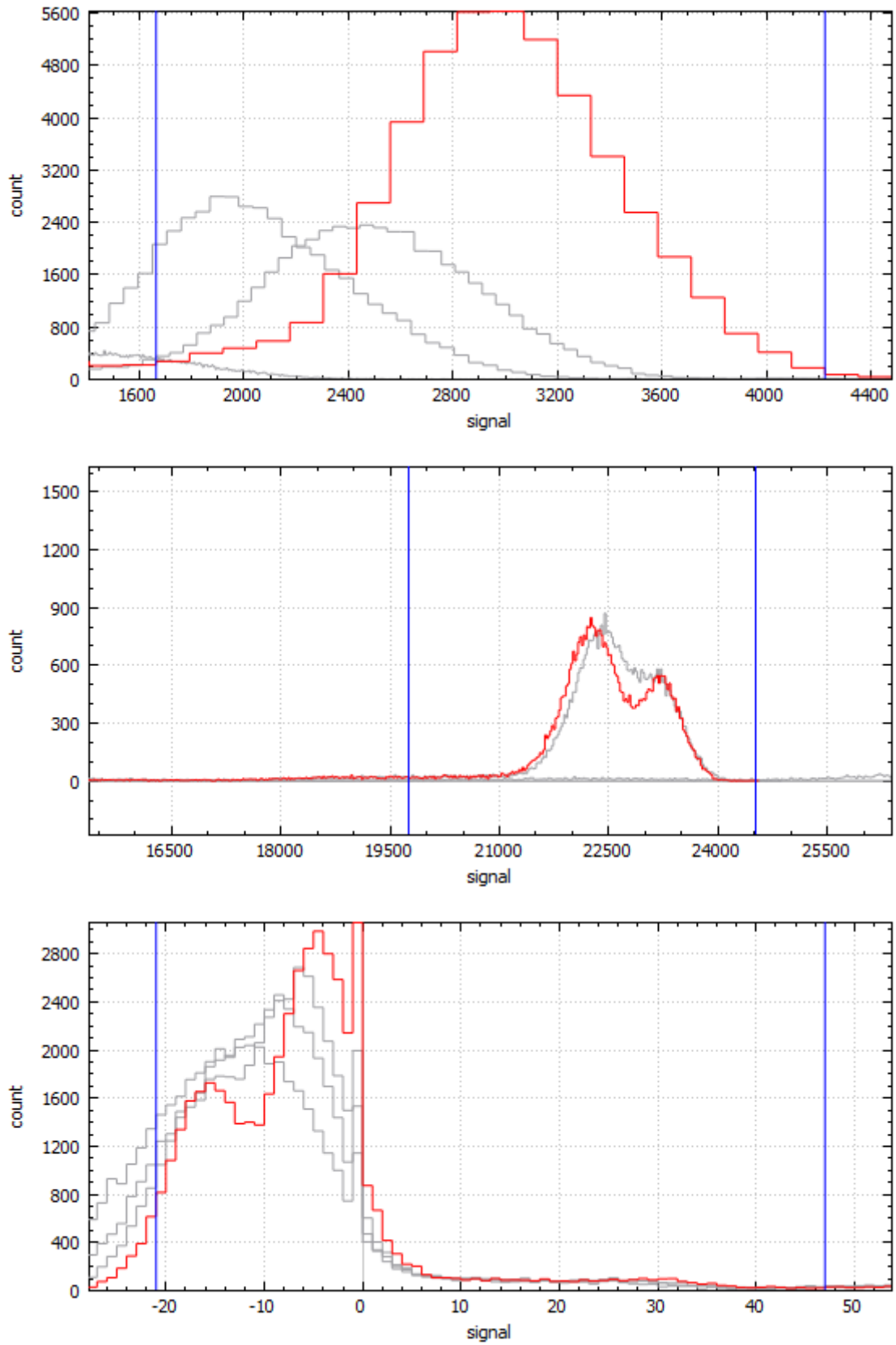


Figure 14: Comparison of the histograms of corrections on an X-ray image of a leaf. Top: Uncorrected image. Middle: Result after flat field correction. Bottom: Result after signal to thickness conversion.

### 5.2.2 Flower

The flower in figure [15] has both thin and thick structures. The image produced with the signal to thickness conversion shows more detail in the thinner regions of the petals and the stamen. In the core of the flower, no real difference can be seen.

The histograms in figure [16] do show a difference in the core. The histogram of the flat field correction flattens when it reaches the thicker structures, whereas the histogram of the signal to thickness conversion shows a peak. Also notable is the very sharp peak in the third histogram that corresponds to the fine structure within the petals.

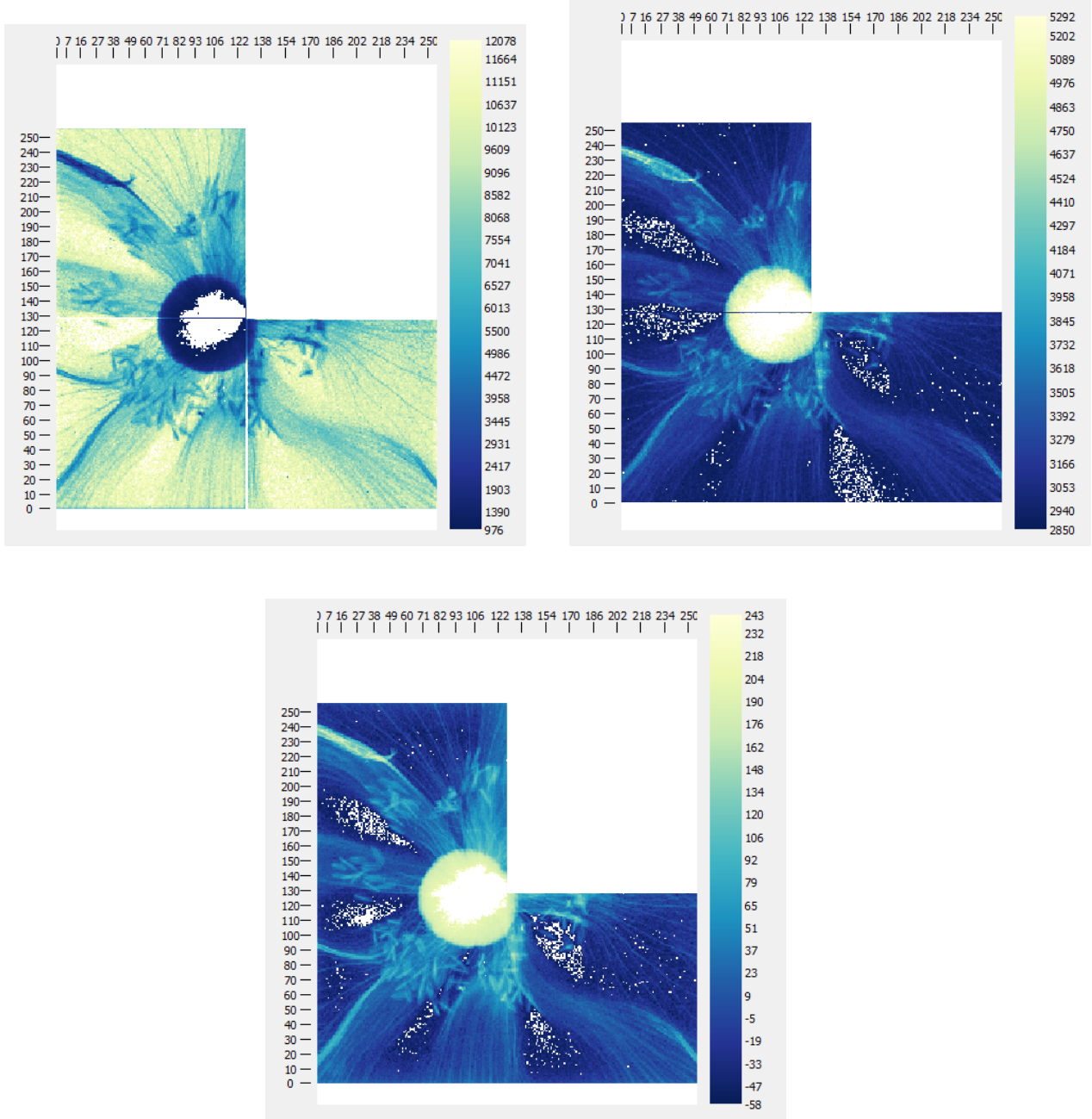


Figure 15: Comparison of corrections on X-ray image of a leaf. Top left: Uncorrected image. Top right: Result after flat field correction. Bottom: Result after signal to thickness conversion.



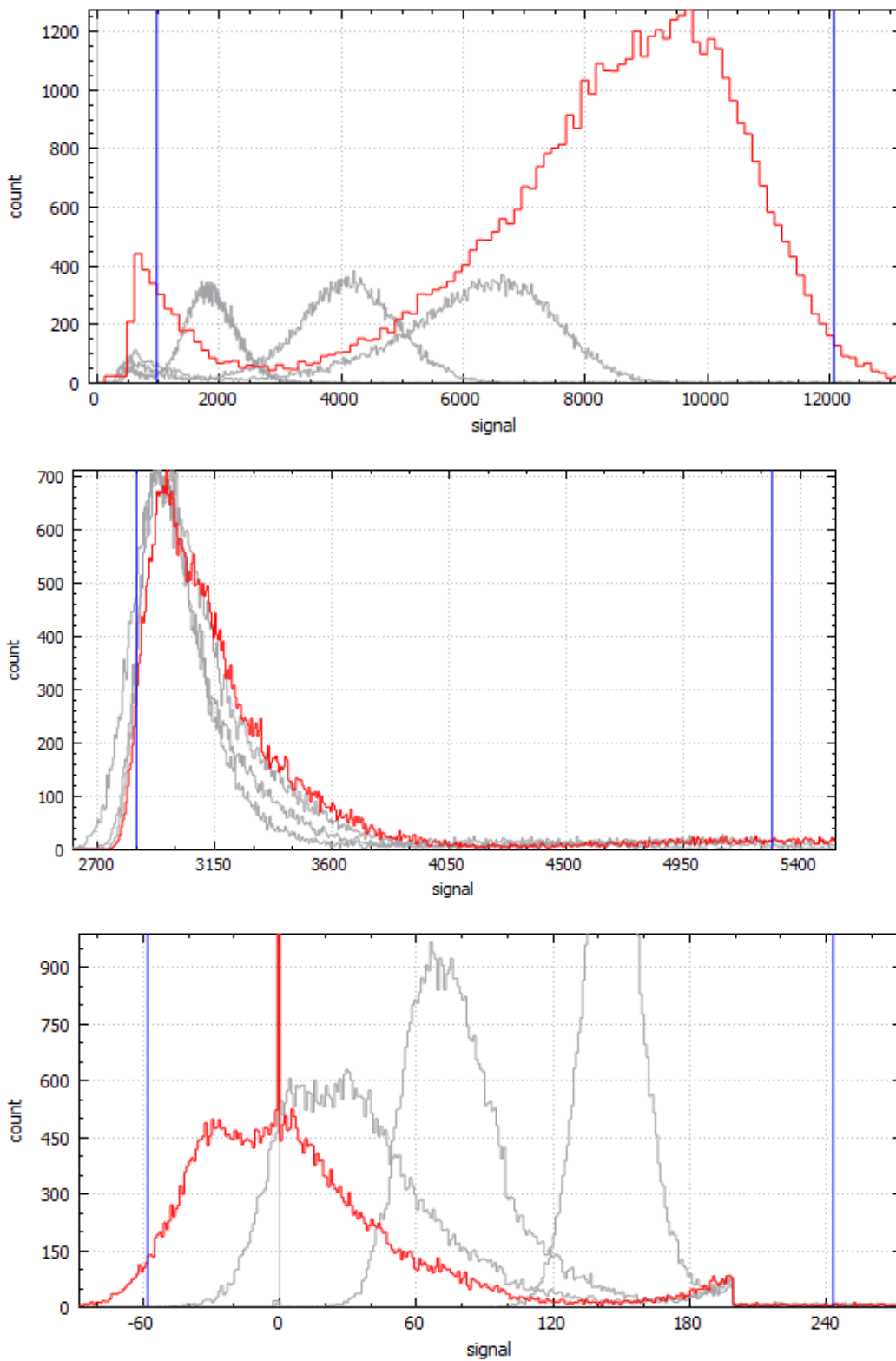


Figure 16: Comparison of the histograms of corrections on an X-ray image of a flower. Top: Uncorrected image. Middle: Result after flat field correction. Bottom: Result after signal to thickness conversion.

### **5.2.3 Composition**

In the composition, shown in figure [17], the leaf is very thin compared to the mushroom and the berries. Because the images don't have a high dynamic range, the leaf is hardly visible. Visually comparing the two corrections does not yield much.

The histograms shown in figure [18] show a large peak that corresponds to the very thin structures of the leaf. After corrections have been applied, this peak splits into two. The broader peak that corresponds to the thicker structures of the mushroom and the berries also splits into two peaks after the signal to thickness conversion.

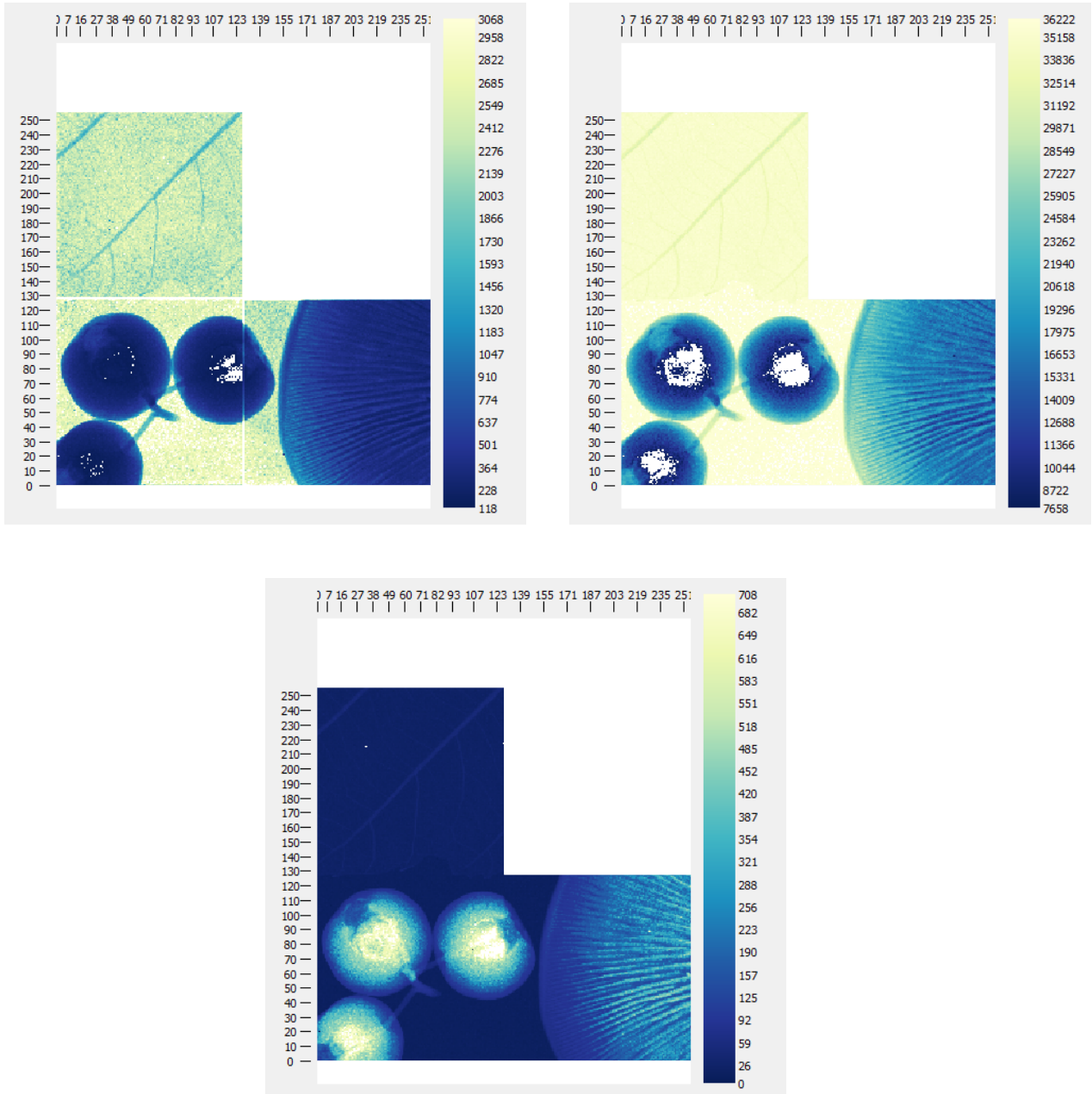


Figure 17: Comparison of corrections on X-ray image of a leaf, a mushroom and three berries. Top left: Uncorrected image. Top right: Result after flat field correction. Bottom: Result after signal to thickness conversion.

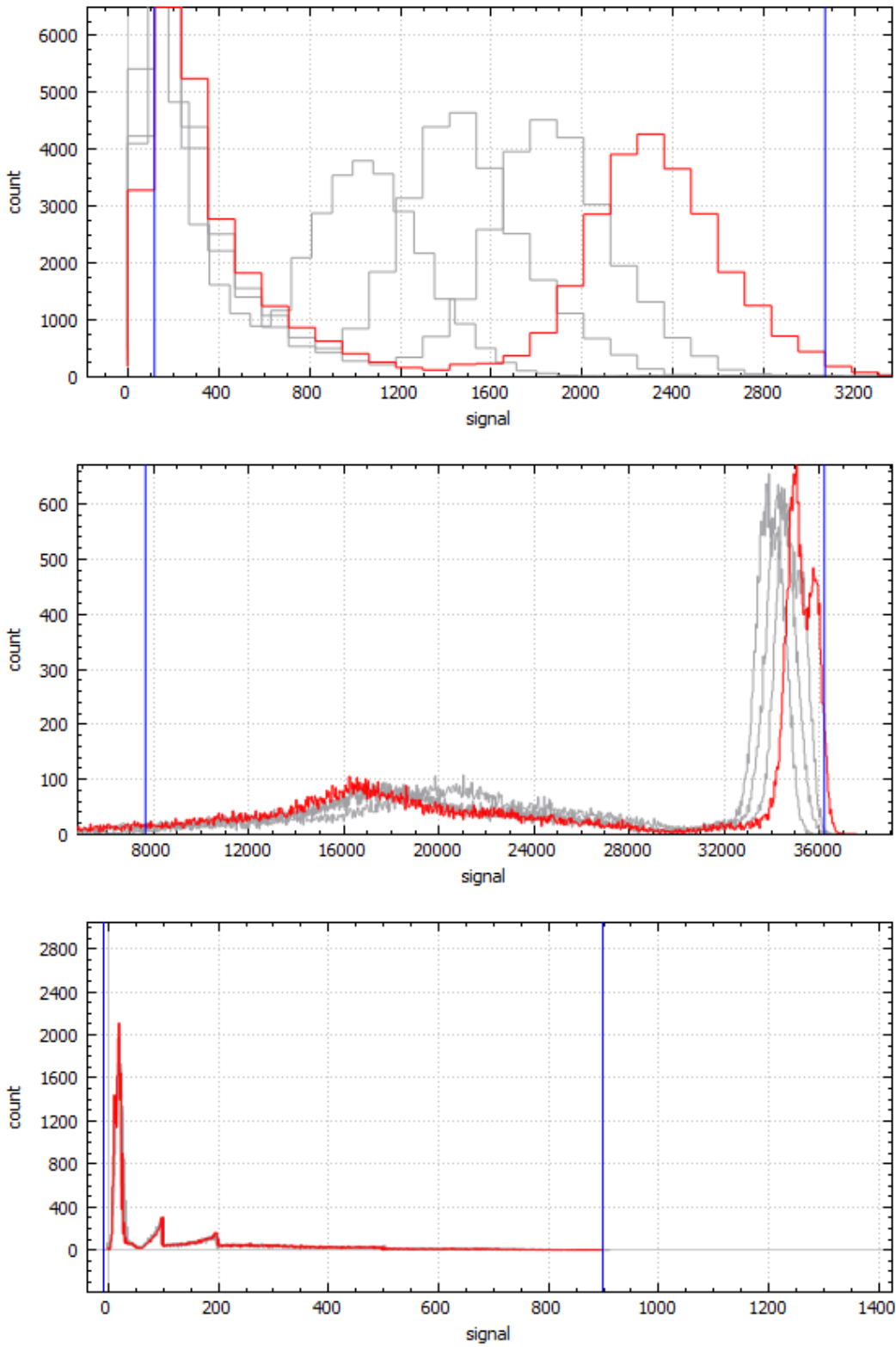


Figure 18: Comparison of the histograms of corrections on an X-ray image of a leaf, a mushroom and three berries. Top: Uncorrected image. Middle: Result after flat field correction. Bottom: Result after signal to thickness conversion.

## 6 Conclusion

A beam hardening correction has been successfully developed using a signal to thickness conversion. Using this correction, the quality of X-ray images that were taken has improved, both in general as well as compared to a flat field correction.

### 6.1 Discussion

The general structure of the software is functional and delivers correct results. There is still room for improvement. Most notably, the signal to thickness conversion currently uses linear interpolation for the signal to thickness conversion. This reduces the quality of the produced images, though it is unclear how large the effect is.

Currently, all flat field corrections have been produced using aluminum sheets. Aluminum resembles neither the organic tissue that was used to test the setup nor breast tissue. Because of this, the corrections do not fully remove the beam hardening artifacts. It would be interesting to test flat field corrections made with a material that more closely resembles organic tissue, for instance glass.

The future outlook for the spectral mammography project is the detection of certain elements or compounds based on their spectral behaviour.

## References

- [1] T. Balakumaran, I.L.A. Vennila, C. Gowri Shankar, *Detection of Microcalcification in Mammograms Using Wavelet Transform and Fuzzy Shell Clustering*, IJCSIS, 2010
- [2] B. Wallet, J. Solka, C. Priebe, *A Method for Detecting Microcalcifications in Digital Mammograms*, J Digit Imaging, 1997
- [3] R. Ballabriga, M. Campbell, E. Heijne, X. Llopart, L. Tlustos, W. Wong, *Medipix3: A 64 k pixel detector readout chip working in single photon counting mode with improved spectrometric performance*, Nucl. Instr. and Meth. 2010
- [4] J. Bushberg, J. Seibert, E. Leidholdt Jr., J. Boone, *The Essential Physics of Medical Imaging, Second Edition* 2002
- [5] M. van Beuzekom, *Speedy Pixel Detector Readout module*, <https://wiki.nikhef.nl/detector/Main/SpiDr>
- [6] E. Schioppa, *The Color of X-rays*, 2014
- [7] The Shoe Fitting Fluoroscope, <http://www.orau.org/ptp/collection/shoefittingfluor/shoe.htm>
- [8] J. Hubbel, S. Seltzer, *Tables of X-Ray Mass Attenuation Coefficients and Mass Energy-Absorption Coefficients from 1 keV to 20 MeV for Elements Z = 1 to 92 and 48 Additional Substances of Dosimetric Interest*, NIST Standard Reference Database, 1996 - 2014
- [9] C. Grupen, B. Schwartz, *Particle Detectors*, 2008
- [10] R. Evans, *The Atomic Nucleus*, 1955
- [11] Lawrence Berkeley National Laboratory, *X-ray Data Booklet*, 2009
- [12] J. Jakubek, *Beam hardening correction*. <http://aladdin.utef.cvut.cz/ofat/methods/BeamHardening/BeamHardening.html>
- [13] The QT Library. <http://www.qt.io/about-us/>
- [14] Spline interpolation open source library. <http://kluge.in-chemnitz.de/opensource/spline/>